Materials Advances

ROYAL SOCIETY OF CHEMISTRY

PAPER

View Article Online
View Journal | View Issue

Cite this: *Mater. Adv.*, 2024, 5, 5140

Enhanced gas sensing performance of sprayed ZnO–$ZnWO_4$ toward CO gas

Mohamed H. Sayed,[ab] Tina Dilova,[c] Genoveva Atanasova,[c] Georgi Avdeev,[d] Mostafa Boshta,[a] Anna Og. Dikovska[e] and Mohammed M. Gomaa *[a]

Received 7th February 2024,
Accepted 29th April 2024

DOI: 10.1039/d4ma00121d

rsc.li/materials-advances

Composite ZnO–$ZnWO_4$ films were obtained by a cost-effective chemical spray pyrolysis approach on a glass substrate using zinc chloride and ammonium metatungstate as starting precursors. The X-ray diffraction investigation indicated that the crystal structure of the obtained films was a composition of ZnO and $ZnWO_4$ phases with the predominant $ZnWO_4$ phase. Scanning electron microscopy images for sprayed mixed ZnO–$ZnWO_4$ layers exhibit a porous structure. Gas sensing performance was tested for detecting carbon monoxide (CO) at different operating temperatures. It was found that the sprayed composite ZnO–$ZnWO_4$ layer shows a maximum sensitivity of 422.7% for 30 ppm CO at 250 °C with good sensor performance. This study suggests that the sprayed ZnO–$ZnWO_4$ composite layer is a good candidate material for CO detection at a relatively low operating temperature.

Introduction

Gas sensors play a pivotal role in modern society by detecting and monitoring various gases in the environment, contributing to safety, environmental protection, and industrial processes. The scientific and economic communities are beginning to pay more attention to this issue. Numerous dangerous gases, including carbon monoxide (CO) ammonia (NH_3), VOCs, and others, are released during our daily activities.[1] Exposure to toxic gases at concentrations exceeding established thresholds can lead to both immediate and long-term health hazards for humans.[2] Among poisonous gases, carbon monoxide (CO) is one of the most common and dangerous gases that can harm the human body's respiratory system.

Carbon monoxide (CO) is a colorless, odorless gas that is produced during the incomplete combustion of carbon-containing fuels. It is crucial to have functional CO sensors installed in homes, workplaces, and any other area where carbon-based fuels are used to prevent exposure to the gas. Many researchers have tried to fabricate different kinds of gas sensors in order to detect harmful gases effectively.[3–12] Metal oxide-based sensors have gathered significant attention among gas sensors due to their effective sensing characteristics.[13]

WO_3 and ZnO stand out among metal oxide semiconductors (MOSs) as potential materials for gas sensing applications, capable of detecting a wide variety of oxidizing and reducing gases.[14] Metal oxide gas sensors often need to be used at quite high temperatures, typically about 350 °C or more. Additionally, MO sensors still have a few issues such as selectivity and humidity dependence. As a result, current research focuses heavily on decreasing the working temperature of gas sensors in order to meet the requirements for decreased power consumption, safety, and use in a variety of industrial applications. This endeavor has resulted in the creation of innovative active sensing materials with the goal of achieving strict criteria for improved sensing performance, such as fast response, low power consumption, and high repeatability.[15] In this regard, various strategies for improving the gas detection performance of metal oxide films have been developed, including morphological control,[16] metal doping,[17,18] and defect density.[19] Metal doping, also known as composite preparation, is an important step in the synthesis process that has been widely utilized to modify the characteristics of oxides, such as lattice structure, electronic structure, and lattice defects, and modulate their applications.[20] Many metallic and nonmetallic elements have been doped into WO_3 to produce lattice defects, increase oxygen vacancies, modify the band gap, or form impurity levels in the band gaps, resulting in dramatically improved sensing characteristics.[21]

Recently, improved gas sensing performance has been achieved by employing innovative mixed-metal oxides that benefit from the synergistic effects of the two different oxide

[a] *Solid State Physics Department, National Research Centre, Dokki 12622, Giza, Egypt. E-mail: dr.metwalyg@gmail.com*
[b] *Molecular and Fluorescence Spectroscopy Lab., Central Laboratories Network, National Research Centre, Dokki 12622, Giza, Egypt*
[c] *Institute of General and Inorganic Chemistry, Bulgarian Academy of Sciences, Acad. G. Bonchev str., bl. 11, Sofia 1113, Bulgaria*
[d] *Rostislaw Kaischew Institute of Physical Chemistry, Bulgarian Academy of Sciences, Acad. G. Bonchev str., bl. 11, Sofia 1113, Bulgaria*
[e] *Institute of Electronics, Bulgarian Academy of Sciences, 72 Tsarigradsko Chaussee, Sofia 1784, Bulgaria*

compositions.[13] Mixed metal oxides or metal oxide composites are a viable strategy for enhancing the physical properties of gas sensors, such as sensitivity, selectivity, stability, and other essential parameters of the fabricated sensor.[22–24] Mixed metal oxides are a great process in addressing the rising need for precise and reliable gas sensing solutions in a variety of industries due to their versatility and adaptability. The combining of metal oxides in the right proportion is a beneficial method for improving gas-sensing performance.[14]

In recent years, there has been a significant focus on developing novel mixed oxides rather than traditional mixed binary oxides, such as tungstate, ferrites, cobaltates, and stannates.[25,26] Zinc tungstate ($ZnWO_4$) belongs to the metal tungstate family and exhibits significant potential in a range of applications, such as photoluminescence, microwave technologies, optical fibers, and environmental applications.[27,28] Numerous studies have demonstrated the efficiency of composite materials in gas sensing applications, implying that enhanced performance can be achieved by the synergistic interaction between different metal oxides.[29–33] In principle, mixing different semiconductor oxides can reduce their band gap, increase electron–hole pair separation, and lead to enhanced thermal dynamic stability and gas sensing activity.[34–37]

In this study, we effectively synthesized and evaluated pure ZnO and a new composite metal oxide (ZnO–$ZnWO_4$) composed of zinc tungstate ($ZnWO_4$) and zinc oxide (ZnO) phases. The composite was fabricated for detecting low concentrations of CO gas in the environment. To our knowledge, there are no documented cases in the literature of ZnO–$ZnWO_4$ thin film synthesis using the cost-effective chemical spray pyrolysis (CSP) approach. This approach is especially useful since it allows for the deposition of homogeneous oxide materials across wide areas of the substrate, while maintaining a low deposition temperature. The obtained results show that the fabricated ZnO–$ZnWO_4$ based sensor has a high sensitivity and selectivity to CO gas compered to sprayed pure ZnO films, making it suitable for applications such as workplace safety management and monitoring air quality. As far as we are aware, this is the first investigation into the detecting capabilities of a sprayed ZnO–$ZnWO_4$ composite-based sensor toward CO gas. This composite is highly stable and efficient at moderate temperature.

Methods and materials

Sample fabrication

Pure ZnO and a composite of the ZnO–$ZnWO_4$ films were synthesized by a chemical spray pyrolysis approach (CSP) using an aqueous solution of zinc chloride ($ZnCl_2$ Sigma Aldrich) and ammonium metatungstate ($(NH_4)_6H_2W_{12}O_{40}{\cdot}xH_2O$ Sigma Aldrich). The initial precursor for deposition of pure ZnO thin films was a 0.1 M aqueous solution of zinc chloride. A combined solution of 0.1 M aqueous zinc chloride and 0.1 M ammonium metatungstate was used to provide clear solutions suitable for spraying composite ZnO–$ZnWO_4$ films. Prior to the deposition process, the glass substrate was cleaned using acetone in an ultrasonic bath for 20 minutes, followed by rinsing with deionized water and alcohol. To achieve highly controlled and uniform films, the starting solution was atomized into fine droplets using an automatic spray atomizer onto the heated glass substrate at 480 °C. For all deposited samples, the deposition duration, compressed air pressure, and distance between the nozzle and the substrate were held constant at 10 minutes, 1.5 bar, and 30 cm, respectively. The sprayed process of the nanostructured ZnO–$ZnWO_4$ composite layer and their gas sensing test is presented schematically in Fig. 1.

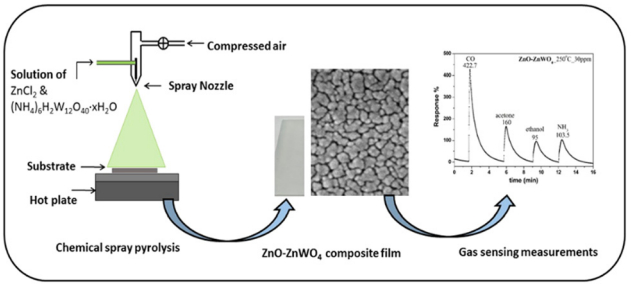

Fig. 1 Schematic description of spraying of the ZnO–$ZnWO_4$ composite layer.

Material characterization

The crystalline structure and phase composition of the sprayed samples were investigated using X-ray diffraction (XRD) on an Empyrean diffractometer (PANalytical). The quantitative phase composition of the samples was obtained after profile fitting of the presented phases by using a HighScore Plus and ReX Software. Raman measurements were performed using a confocal Raman microscope, model WITec Alpha 300 RA, under 532 nm laser radiation. The surface morphology of the sprayed pure ZnO and ZnO–$ZnWO_4$ composite layers were studied using scanning electron microscopy (FIB-SEM) with Scios 2 DualBeam (Thermo Fisher) equipment. X-ray photoelectron spectroscopy (XPS) using an AXIS Supra electron spectrometer (Kratos Analytical Ltd., Manchester, UK) was used to investigate the chemical composition of the deposited samples.

Sensor fabrication

The sensor elements were fabricated as Au electrodes were evaporated on the top of the samples (with thickness of 300 nm and 3 mm gap between them). The sensor element was placed on a resistive heater in a test chamber. The gas sensor measurements were performed in a homemade test chamber at different temperatures in the range of 25–250 °C. High-purity N_2 was used as a reference gas at a flow rate of 55 sccs (standard cubic centimeters per second). The test gases: carbon monoxide (CO), acetone ($(CH_3)_2CO$), ethanol (C_2H_6O), and ammonia (NH_3) were injected by a microsyringe into the chamber for one second to reach a concentration of 30 ppm. The gas sensing response properties were followed by monitoring the variation of the sensor's resistance as measured by a Fluke 8845A multimeter and recorded in real time by a PC. The gas response was estimated by calculating the ratio $\Delta R/R_a$ (%) as

the following formula:

$$S\,(\%) = \frac{|R_a - R_g|}{R_a} \times 100\% \quad (1)$$

where R_a is the sample resistance in the reference gas, $\Delta R = (R_g - R_a)$, R_g being the sample resistance in the test gas. The response time is defined as the time needed to reach 90% of the maximum gas response after the gas is turned on; and the recovery time is the time needed for the response to fall down to 10% of its maximum once the gas is turned off.

Results and discussion

Structural properties

In Fig. 2, the XRD patterns of the pure ZnO and mixed ZnO–$ZnWO_4$ layers are presented. Fig. 2(a) shows the XRD pattern of the prepared ZnO thin films. The indexed peaks of the deposited films correspond to the hexagonal structure of zinc oxide, which fits well with data of JCPDS reference pattern No. 98-006-7849. As seen, the deposited ZnO layer has a polycrystalline structure with a preferential orientation in the (002) plane. The XRD patterns of the mixed ZnO–$ZnWO_4$ composite are presented in Fig. 2(b). The sample structure represents a composition of ZnO and $ZnWO_4$ phases (monoclinic, JCPDS No. 98-008-4540). The estimated ratio between the two crystalline phases ZnO/$ZnWO_4$ is 8.5 to 91.5%, respectively. It could be concluded that the sample presents a composite structure consisting of ZnO and $ZnWO_4$ phases, as the $ZnWO_4$ is the predominant phase. We named this composite system ZnO–$ZnWO_4$. It should be noted that the XRD analyses were performed after deposition of Au electrodes, and consequently the peaks of Au were also identified in the patterns, as shown in Fig. 2(a) and (b).

Furthermore, Raman spectroscopy was used to identify the crystal structure and structural defects of the deposited samples. Fig. 3(a) shows the Raman spectral measurement of the pure sprayed ZnO layer. The peaks at 94 cm^{-1} and 433 cm^{-1} matched the E_2(low) and E_2(high) fundamental phonon modes of ZnO with a hexagonal wurtzite structure, respectively. These phonon modes in the Raman spectra, E_2(low) and E_2(high), indicate well-formed ZnO crystals. Additionally, the intensity of these phonon modes is strongly related to the ZnO crystal quality. The peak at 552 cm^{-1} corresponds to A_1(LO), which is attributed to the existence of oxygen vacancies and Zn interstitials in the ZnO lattice. The peak at 1094 cm^{-1} corresponding to the multiple phonon process of E_1(LO) originates

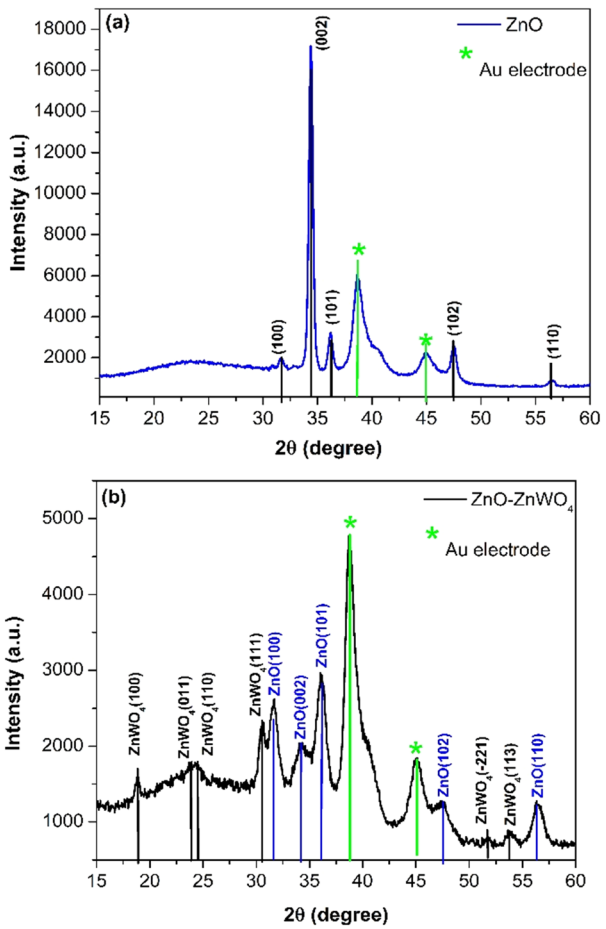

Fig. 2 X-ray diffraction patterns of sprayed (a) ZnO and (b) ZnO–$ZnWO_4$ composite layers.

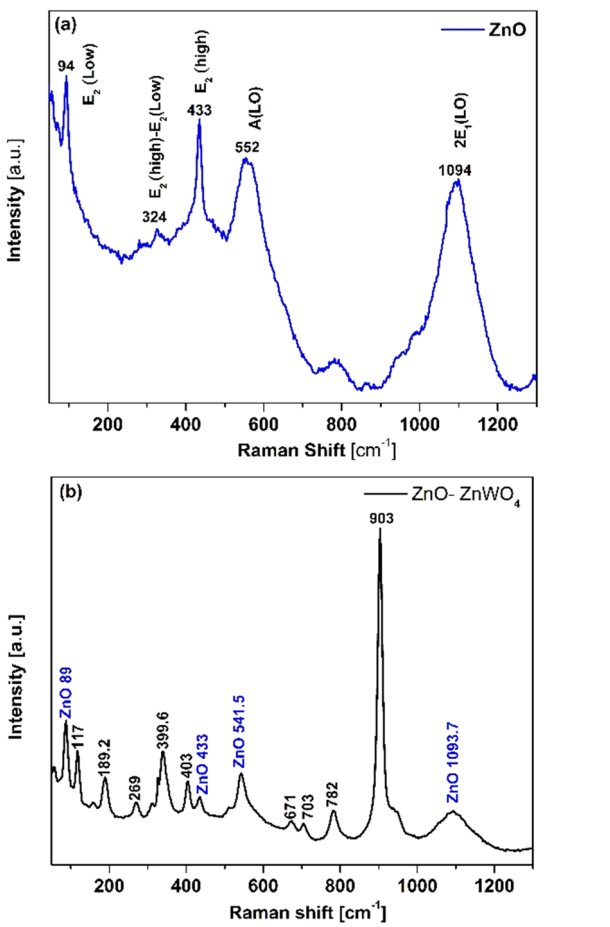

Fig. 3 Raman spectra of sprayed (a) ZnO and (b) ZnO–$ZnWO_4$ composite layers.

due to the lattice vibration. The peak that appeared at 324 cm^{-1} was assigned to E_2(high)–E_2(low) multiphonon scattering.

In the case of ZnO–$ZnWO_4$ films, the main mode (A_g) is related to the significant peak located at about 903.3 cm^{-1}, which corresponds to the symmetric stretching of W–O bonds. As shown in Fig. 3(b), the Raman B_g and A_g modes at 782 and 703 cm^{-1}, respectively, are connected with the asymmetric stretching of W–O bonds. Furthermore, the Raman A_g and B_g modes at 671, 542, 510, and 402 cm^{-1} are ascribed to long W–O bond stretching modes. Lower intensity modes around 117 (A_g) and 189 (B_g) are associated with the symmetric stretching of O–Zn bonds, whereas the modes at 311 cm^{-1} and 269 cm^{-1} are associated with cationic sublattice vibrations, as illustrated in Fig. 3(b).[38] Additionally, the deposited sample presents all ZnO peaks with a small Raman shift. As a result, all of the vibration modes shown in Fig. 3(b) are distinct and well defined, indicating that the ZnO–$ZnWO_4$ composite has a crystalline structure. The phase structure is efficiently identified as a wolframite-type monoclinic $ZnWO_4$ structure linked with a hexagonal wurtzite ZnO structure by combining comprehensive data from XRD and Raman spectroscopy. The obtained results indicate the successful deposition of the ZnO–$ZnWO_4$ composite using chemical spray pyrolysis.

Surface morphology

SEM images of the prepared ZnO and ZnO–$ZnWO_4$ thin films are shown in Fig. 4. Generally, the SEM analyses reveal that the prepared ZnO and ZnO–$ZnWO_4$ films have crack/hole-free surfaces.

The samples have a granular morphology with an irregular grain shape. The SEM image of the ZnO films and the grain size distribution are shown in Fig. 4(a). The size of the grains was determined with the approximation that they are spherically shaped and their maximum Ferret's diameter was measured. As seen, the size of the grains is in the range of 20–150 nm as the mean Ferret's size is 70 nm. The SEM image of the ZnO–$ZnWO_4$ film shows a surface morphology consisting of smaller grains compared to the ZnO film (Fig. 4(b)). The size of the grains is between 20 and 110 nm with mean Ferret's size of 54 nm. The small grains of the ZnO–$ZnWO_4$ layer contribute significantly to the active surface area and therefore was expected to have a superior sensing performance.[39] The small grains within the ZnO–$ZnWO_4$ layer play an important role in increasing the active surface area. As a result, it was expected that ZnO–$ZnWO_4$ composite would result in enhanced gas sensing performance.

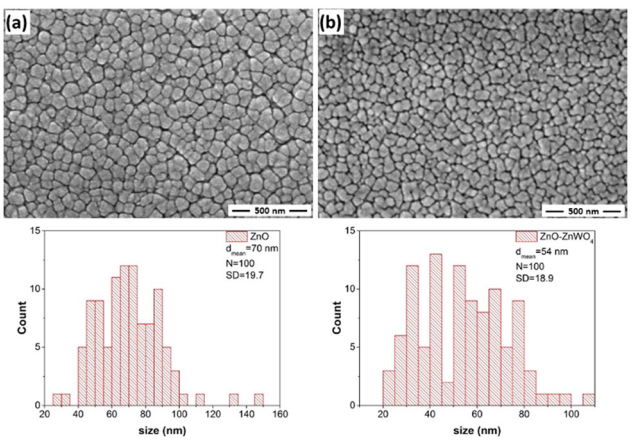

Fig. 4 SEM micrographs of sprayed (a) ZnO and (b) ZnO–$ZnWO_4$ composite layers.

Chemical state and surface composition

Fig. 5 shows the XPS spectra of the Zn 2p, W 4f and O 1s core levels of the pure ZnO and composite ZnO–$ZnWO_4$ samples. The Zn $2p_{3/2}$ and Zn $2p_{1/2}$ peaks of the pure ZnO sample are located at 1021.7 eV and 1044.8 eV, respectively, with a spin–orbit splitting of 23.1 eV. The spin–orbit splitting observed, the binding energy positions and the width of the Zn 2p peaks allow us to conclude that the Zn atoms were in the Zn^{2+} oxidation state.[40]

The broad Zn 2p peak of the composite ZnO–$ZnWO_4$ sample is asymmetric and could be deconvoluted into two components at 1021.7 eV and 1023.2 eV. The main peak at 1021.7 eV can be considered due to Zn in ZnO. The W $4f_{7/2}$ and W $4f_{5/2}$ peaks of the ZnO–$ZnWO_4$ sample are located at 35.6 eV and 37.7 eV (Fig. 5). The binding energies of W $4f_{5/2}$ (35.6 eV) and Zn 2p (1023.2 eV) correspond to $ZnWO_4$.[41] The estimated Zn/W ratio is 3.6. The asymmetric O 1s peak points to the presence of different oxygen-containing species. This peak could be deconvoluted into three components at nearly 530.3 eV, attributed to lattice O^{2-} ions in the metal oxides (O–Zn,W); at 531.1 eV, associated with oxygen vacancies (O def); and at 532.2 eV, attributed to the presence of adsorbed hydroxyl, carbonate or O_2 species (O ads).[42] It should be noted that the presence of defects on the surface of the composite sample is slightly higher than on the surface of the pure ZnO.

Gas sensing properties

The working temperature is one of the main parameters that determine the response of a gas sensor, since it controls the processes of adsorption and desorption of the different gas species existing in the surrounding atmosphere on the surface.[43] Therefore, we focused our attention on the temperature dependence of the gas response of the as-prepared sensor elements under a concentration of 30 ppm of CO gas. The gas responses of the ZnO and ZnO–$ZnWO_4$ sensors at different working temperature are presented in Fig. 6. No sensor reaction of the pure and composite samples was detected at room temperature independently of the gas exposure. The samples started working as sensor elements as the sensor was heated to a temperature of 100 °C. As seen from Fig. 6, the response of the composite ZnO–$ZnWO_4$ sample for the target gas is substantially higher than the response of the pure ZnO. A slight increase of the working temperature to 150 °C does not actually change the response of the ZnO sample. Further increase of the working temperature continues the tendency of increasing the response of both sensors. Obviously, more significant reaction to the gas components was demonstrated by the composite ZnO–$ZnWO_4$ sensor (Fig. 6). The highest response was

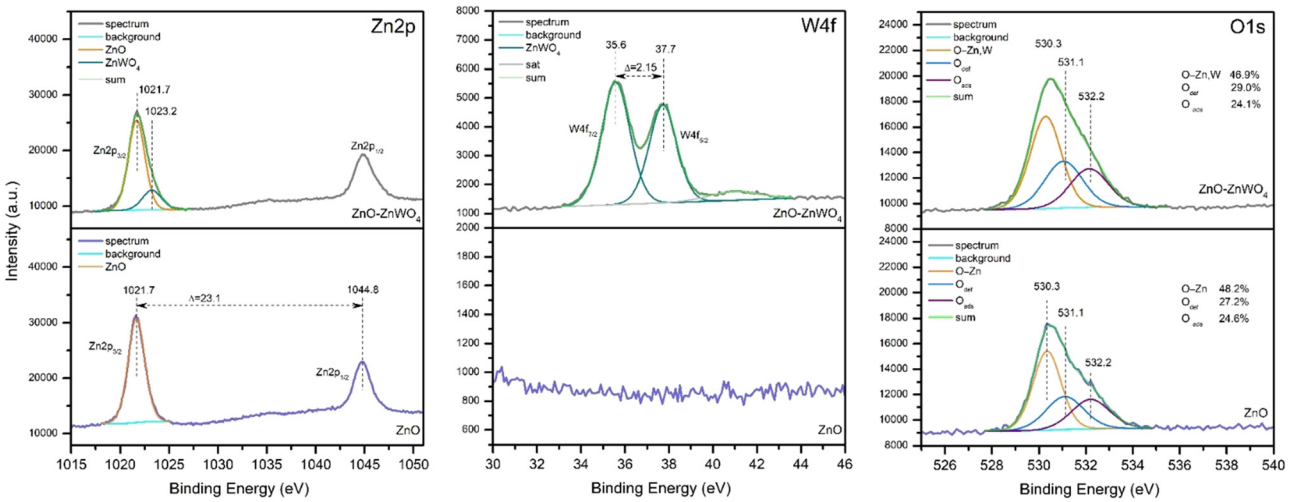

Fig. 5 XPS spectra of sprayed ZnO and ZnO–$ZnWO_4$ composite layers.

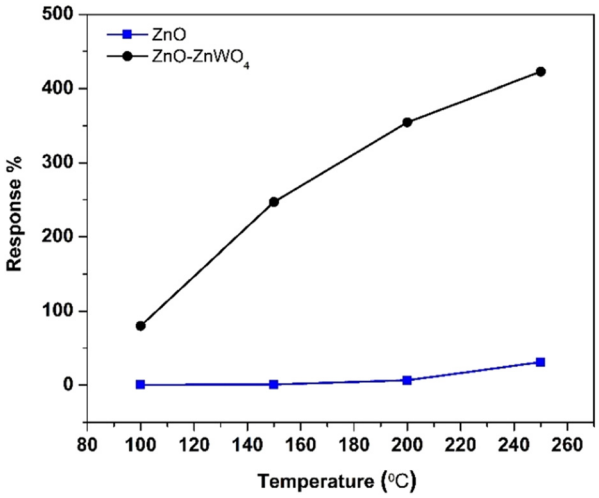

Fig. 6 Response of ZnO and ZnO–$ZnWO_4$ sensors at different temperatures toward 30 ppm CO gas.

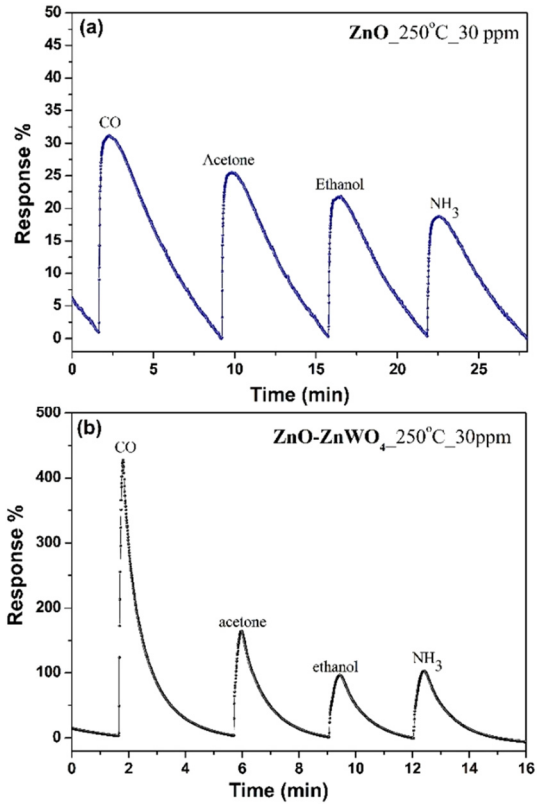

Fig. 7 Dynamic response of (a) ZnO and (b) Zn–$ZnWO_4$ sensors at 250 °C and 30 ppm.

demonstrated by both sensor elements at 250 °C temperature, which was then used as the operating point for all further measurements of the fabricated sensors.

As shown in Fig. 7, the dynamic curves of the fabricated sensors show a recovery to the primary baseline value when venting the tested gas, indicating good reversibility of the sensors. The dynamic response of the ZnO sensor enhances in a similar way for all gases as shown in Fig. 7(a), while for the ZnO–$ZnWO_4$ sensor the enhancement is predominantly to CO exposure as shown in Fig. 7(b). The response of the ZnO–$ZnWO_4$ sensor is 13 times higher than the one of the ZnO sensor. This result is probably related mainly to the composite structure of the ZnO–$ZnWO_4$ sensor with smaller grain morphology and more oxygen deficiency stage on the surface compared to that of the ZnO sensor. The enhanced gas sensor response of the composite sensor element could be associated with the formation of *n*–*n* heterojunctions.[2] Moreover, the synergistic behaviour that can take place in heterostructured composite materials should be taken into consideration as an additional mechanism to improve the gas sensing efficacy.[2]

The gas sensor response is explained by the resistance change of the sensing film, which mainly occurs due to gas adsorption and desorption on the surface of the sensing film. The CO sensing mechanism of the ZnO–$ZnWO_4$ sensor is

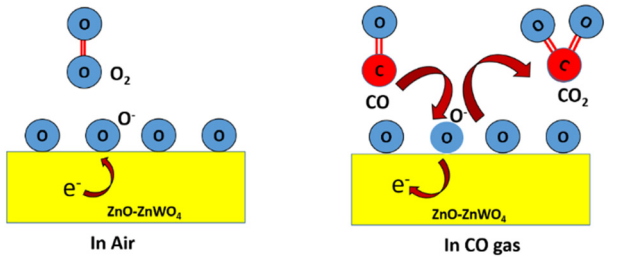

Fig. 8 CO sensing mechanism of the ZnO–$ZnWO_4$ composite layer.

schematically shown in Fig. 8. Oxygen species (O^{-2}, O^{-}, and O^{2-}) are formed according to the operating temperature after capturing the electrons from the sensing materials. The outcome is a reduction in the concentration of oxygen at the surface and release of electrons that are initially trapped, thereby decreasing the resistivity of the gas sensor material.[44] The reaction that occurs due to gas adsorption on the surface of the sensing material is described by the following equation.[45]

$$CO(gas) + O^{-}(gas) \rightarrow CO_2(gas) + e^{-} \quad (2)$$

Gas selectivity is a very important parameter for gas sensors and was investigated for the fabricated sensors by comparing the measurable parameters for each analyzed gas at the same concentration level. Fig. 9 shows the sensor responses of the fabricated sensors towards different gases; CO, acetone, ethanol, and ammonia (NH_3) with 30 ppm concentration at a working temperature of 250 °C. The selectivity of the pure ZnO sensor Fig. 9(a) is substantially lower compared to the one of the ZnO–$ZnWO_4$ sensor Fig. 9(b) and the ZnO–$ZnWO_4$ sensor is showing high selectivity towards CO gas.

According to the gas sensing properties of the samples, another important parameter is the time needed for the sensor element to react under gas exposure. Generally, it was found that increasing the operating temperature, the response and recovery times of the pure ZnO and ZnO–$ZnWO_4$ composite sensors decrease for all tested gases.

In Fig. 10, the dependence of the response and recovery time of the ZnO–$ZnWO_4$ composite sensor on the working temperature under CO exposure is shown. As seen, increasing the working temperature substantially decreases the time for the sensor response and recovery.

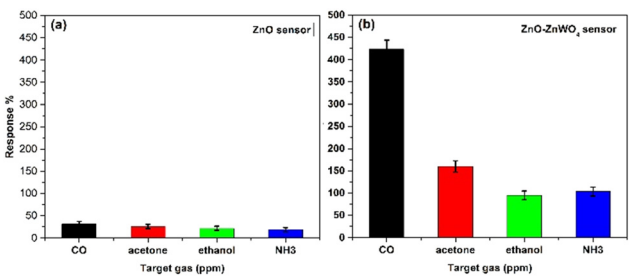

Fig. 9 Selectivity histogram of (a) ZnO and (b) ZnO–$ZnWO_4$ sensors operated at 250 °C for different gases.

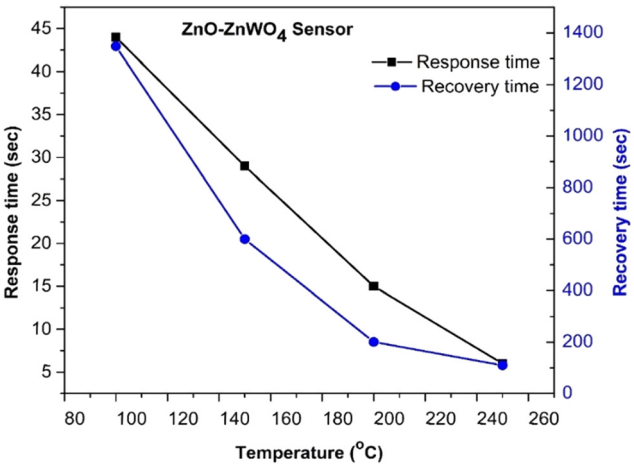

Fig. 10 Response and recovery time of the ZnO–$ZnWO_4$ sensors at different temperatures toward 30 ppm CO gas.

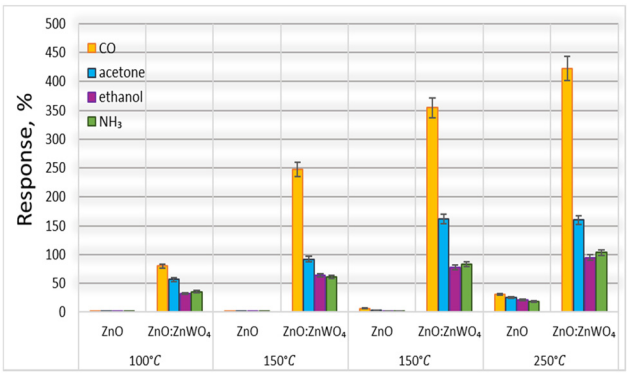

Fig. 11 Comparison of the gas performance of the ZnO and ZnO–$ZnWO_4$ sensors at different working temperatures and gas exposure.

The estimated response and recovery times of the ZnO–$ZnWO_4$ composite sensor at 250 °C temperature under CO exposure are 6 and 110 s, respectively.

It could be concluded that the composite ZnO–$ZnWO_4$ sensor shows superior sensing performance compared to the pure ZnO sensor and the ZnO–$ZnOWO_4$ sensor is predominantly sensitive to CO exposure, as shown in Fig. 11. It should be noted that the increase in the working temperature of the ZnO sensor does not influence its selectivity.

Meanwhile, the selectivity of the ZnO–$ZnWO_4$ sensor to CO is enhanced with increasing the temperature. The best sensor performance, the highest response and selectivity, was obtained by the composite ZnO–$ZnWO_4$ sensor working at 250 °C temperature under CO exposure (Fig. 11).

Conclusions

Sprayed pure ZnO and composite ZnO–$ZnWO_4$ films were utilized to fabricate an efficient gas sensor toward CO detection. The obtained composite ZnO–$ZnWO_4$ films showed polycrystalline structure and the ratio between the two crystalline

phases ZnO/$ZnWO_4$ is 8.5 to 91.5%. The SEM image of the ZnO–$ZnWO_4$ film shows the surface morphology consisting of smaller grains compared to the pure ZnO film, playing an important role in increasing the surface area of the sensor leading to enhanced gas sensing performance. The XPS measurements noted that the presence of defects on the surface of the ZnO–$ZnWO_4$ film is slightly higher than on the surface of the pure ZnO.

The best sensor performance, the highest response and selectivity, was obtained by the composite ZnO–$ZnWO_4$ sensor operating at 250 °C temperature under 30 ppm CO exposure and was 13 times higher than the one of the pure ZnO sensor. The estimated response and recovery times of the composite ZnO–$ZnWO_4$ sensor under CO exposure are 6 and 110 s, respectively. Therefore, based on the obtained results, the fabricated composite ZnO–$ZnWO_4$ sensor can be used for CO detection at low concentrations in future sensor technology.

Author contributions

Mohamed H. Sayed: conceptualization, data curation, formal analysis, investigation, methodology, writing – original draft, writing – review & editing. Tina Dilova: investigation, formal analysis, writing – original draft. Georgi Avdeev: investigation, formal analysis. Genoveva Atanasova: investigation, formal analysis, validation, writing – original draft, writing – review & editing. Mostafa Boshta: conceptualization, resources, supervision, validation, writing – original draft, writing – review & editing. Anna Og. Dikovska: funding acquisition, project administration, resources, conceptualization, investigation, formal analysis, writing – original draft, writing – review & editing. Mohammed M. Gomaa: funding acquisition, project administration, resources, conceptualization, data curation, formal analysis, investigation, methodology, writing – original draft, writing – review & editing.

Conflicts of interest

There are no conflicts to declare.

Acknowledgements

The authors acknowledge the financial support of the bilateral project ASRT-BAS 10120 funded by the Bulgarian Academy of Sciences, Academy of Scientific Research and Technology – Egypt, and the authors from National Research Centre acknowledge the financial support of the in-house fund with project number 13020240.

References

1 K. Wetchakun, T. Samerjai, N. Tamaekong, C. Liewhiran, C. Siriwong, V. Kruefu, A. Wisitsoraat, A. Tuantranont and S. Phanichphant, Semiconducting metal oxides as sensors for environmentally hazardous gases, *Sens. Actuators, B*, 2011, **160**, 580–591.
2 F.-J. Meng, R.-F. Xin and S.-X. Li, Metal Oxide Heterostructures for Improving Gas Sensing Properties: A Review, *Materials*, 2023, **16**, 263.
3 S. M. Majhi, A. Mirzaei, H. W. Kim, S. S. Kim and T. W. Kim, Recent advances in energy-saving chemiresistive gas sensors: A review, *Nano Energy*, 2021, **79**, 105369.
4 G. Jiménez-Cadena, J. Riu and F. X. Rius, Gas sensors based on nanostructured materials, *Analyst*, 2007, **132**, 1083–1099.
5 D. Y. Li, H. Y. Kang, Y. H. Liu, J. Zhang, C. Y. Yue, D. Yan and X. W. Lei, A 0D hybrid lead-free halide with near-unity photoluminescence quantum yield toward multifunctional optoelectronic applications, *Chem. Sci.*, 2023, **15**, 953–963.
6 Y. Zhai, J. Ye, Y. Zhang, K. Zhang, E. Zhan, X. Zhang and Y. Yang, Excellent sensing platforms for identification of gaseous pollutants based on metal–organic frameworks: A review, *Chem. Eng. J.*, 2024, **484**, 149286.
7 B. Jie, H. Lin, Y. Zhai, J. Ye, D. Zhang, Y. Xie, X. Zhang and Y. Yang, Mechanism, design and application of fluorescent recognition based on metal organic frameworks in pollutant detection, *Chem. Eng. J.*, 2023, **454**, 139931.
8 Y. Zhao, H. Lin, M. Chen and D. Yan, Niflumic anion intercalated layered double hydroxides with mechano-induced and solvent-responsive luminescence, *Ind. Eng. Chem. Res.*, 2014, **53**, 3140–3147.
9 R. Gao, D. Cao, Y. Guan and D. Yan, Fast and Reversible Humidity-Responsive Luminescent Thin Films, *Ind. Eng. Chem. Res.*, 2016, **55**, 125–132.
10 R. Gao, X. Fang and D. Yan, Recent developments in stimuli-responsive luminescent films, *J. Mater. Chem. C*, 2019, **7**, 3399–3412.
11 W. Zhai, Y. Chen, Y. Liu, Y. Ma, P. Vijayakumar, Y. Qin, Y. Qu and Z. Dai, Covalently Bonded Ni Sites in Black Phosphorene with electron redistribution for efficient metal-light weighted water electrolysis, *Nano-Micro Lett.*, 2024, **16**, 1–13.
12 R. Gao and D. Yan, Ordered assembly of hybrid room-temperature phosphorescence thin films showing polarized emission and the sensing of VOCs, *Chem. Commun.*, 2017, **53**, 5408–5411.
13 C. Wang, L. Yin, L. Zhang, D. Xiang and R. Gao, Metal oxide gas sensors: Sensitivity and influencing factors, *Sensors*, 2010, **10**, 2088–2106.
14 C. Siriwong, K. Wetchakun, A. Wisitsoraat and S. Phanichphant, Gas sensing properties of WO_3-doped ZnO nanoparticles synthesized by flame spray pyrolysis, *Proc. IEEE Sens.*, 2009, 118–123.
15 A. Kumar, A. Sanger, A. Kumar and R. Chandra, Porous silicon filled with Pd/WO_3-ZnO composite thin film for enhanced H_2 gas-sensing performance, *RSC Adv.*, 2017, **7**, 39666–39675.
16 A. A. Firooz, Effect of different morphologies of nanostructured SnO_2 and their nanocomposites on sensing behavior, *J. Math. Nanosci.*, 2013, **3**, 13–16.
17 S. R. Gawali, V. L. Patil, V. G. Deonikar, S. S. Patil, D. R. Patil, P. S. Patil and J. Pant, Ce doped NiO nanoparticles as selective NO_2 gas sensor, *J. Phys. Chem. Solids*, 2018, **114**, 28–35.

18 R. Sankar Ganesh, V. L. Patil, E. Durgadevi, M. Navaneethan, S. Ponnusamy, C. Muthamizhchelvan, S. Kawasaki, P. S. Patil and Y. Hayakawa, Growth of Fe doped ZnO nanoellipsoids for selective NO_2 gas sensing application, *Chem. Phys. Lett.*, 2019, **734**, 136725.

19 S. Zargouni, L. Derbali, M. Ouadhour, M. Rigon, A. Martucci and H. Ezzaouia, Elaboration and characterization of PVP-assisted NiO thin films for enhanced sensitivity toward H_2 and NO_2 gases, *Ceram. Int.*, 2019, **45**, 5779–5787.

20 A. M. Pineda-Reyes, M. R. Herrera-Rivera, H. Rojas-Chávez, H. Cruz-Martínez and D. I. Medina, Recent advances in ZnO-based carbon monoxide sensors: Role of doping, *Sensors*, 2021, **21**, 4425.

21 C. Dong, R. Zhao, L. Yao, Y. Ran, X. Zhang and Y. Wang, A review on WO_3 based gas sensors: Morphology control and enhanced sensing properties, *J. Alloys Compd.*, 2020, **820**, 153194.

22 S. Park, Enhancement of hydrogen sensing response of ZnO nanowires for the decoration of WO_3 nanoparticles, *Mater. Lett.*, 2019, **234**, 315–318.

23 C. H. Chang, T. C. Chou, W. C. Chen, J. S. Niu, K. W. Lin, S. Y. Cheng, J. H. Tsai and W. C. Liu, Study of a WO_3 thin film based hydrogen gas sensor decorated with platinum nanoparticles, *Sens. Actuators, B*, 2020, **317**, 128145.

24 L. Nie, X. Guo, C. Gao, X. Wu, J. Chen and L. Peng, Effect of ZnO Content on the Optical H_2 Sensing Properties of Porous $Pt/(WO_3)_{1-x}(ZnO)_x$ Films, *J. Electron. Mater.*, 2022, **51**, 6463–6474.

25 Y. Zhao, X. Li, B. Yan, D. Xiong, D. Li, S. Lawes and X. L. Sun, Recent Developments and understanding of novel mixed transition-metal oxides as anodes in lithium ion batteries, *Adv. Energy Mater.*, 2016, **6**, 1–19.

26 Anusha, P. Kumari, P. Poornesh, S. Chattopadhyay, A. Rao and S. D. Kulkarni, Evaluation of Zn:WO_3 thin films as a sensing layer for detection of NH_3 gas, *Micromachines*, 2023, **14**, 1–12.

27 E. Petronijevic, M. Tomczyk, A. Belardini, P. Osewski, P. Piotrowski, M. Centini, G. Leahu, R. L. Voti, D. A. Pawlak, C. Sibilia and M. C. Larciprete, Surprising Eutectics: Enhanced Properties of ZnO–$ZnWO_4$ from Visible to MIR, *Adv. Mater.*, 2022, **35**, 220600.

28 G. He, H. Fan, L. Ma, K. Wang, D. Ding, C. Liu and Z. Wang, Synthesis, characterization and optical properties of nanostructured $ZnWO_4$, *Mater. Sci. Semicond. Process.*, 2016, **41**, 404–410.

29 Y. M. Hunge, A. A. Yadav, B. M. Mohite, V. L. Mathe and C. H. Bhosale, Photoelectrocatalytic degradation of sugarcane factory wastewater using WO_3/ZnO thin films, *J. Mater. Sci.: Mater. Electron.*, 2018, **29**, 3808–3816.

30 S. R. Sriram, S. Parne, V. S. C. S. Vaddadi, D. Edla, P. Nagaraju, R. R. Avala, V. Yelsani and U. B. Sontu, Nanostructured WO_3 based gas sensors: a short review, *Sens. Rev.*, 2021, **41**, 406–424.

31 B. Nam, T. K. Ko, S. K. Hyun and C. Lee, Sensitivities of a 6:4 (by molar ratio) ZnO/WO_3 composite nanoparticle sensor to reducing and oxidizing gases, *Appl. Surf. Sci.*, 2020, **504**, 144104.

32 A. J. T. Naik, I. P. Parkin and R. Binions, Gas sensing studies of a n-n hetero-junction array based on WO_3 and ZnO composites, *IEEE Sens. J.*, 2014, **14**, 3137–3147.

33 B. Nam, T. K. Ko, S. K. Hyun and C. Lee, NO_2 sensing properties of WO_3-decorated In_2O_3 nanorods and In_2O_3-decorated WO_3 nanorods, *Nano Convergence*, 2019, **6**, 40.

34 D. D. Nguyen, D. T. Do, X. H. Vu, D. V. Dang and D. C. Nguyen, ZnO nanoplates surfaced-decorated by WO_3 nanorods for NH_3 gas sensing application, *Adv. Nat. Sci.: Nanosci. Nanotechnol.*, 2016, **7**, 015004.

35 Y. Sun, L. Chen, Y. Wang, Z. Zhao, P. Li, W. Zhang, Y. Leprince-Wang and J. Hu, Synthesis of MoO_3/WO_3 composite nanostructures for highly sensitive ethanol and acetone detection, *J. Mater. Sci.*, 2017, **52**, 1561–1572.

36 J. Sun, L. Sun, N. Han, J. Pan, W. Liu, S. Bai, Y. Feng, R. Luo, D. Li and A. Chen, Ordered mesoporous WO_3/ZnO nanocomposites with isotype heterojunctions for sensitive detection of NO_2, *Sens. Actuators, B*, 2019, **285**, 68–75.

37 S. K. Hyun, B. Nam, T. K. Ko, C. Lee, S. B. Choi and W. I. Lee, Optimal Composition of ZnO/WO_3 Composite Nanoparticle Gas Sensors, *Phys. Status Solidi A*, 2020, **217**, 1–8.

38 P. F. S. Pereira, A. F. Gouveia, M. Assis, R. C. De Oliveira, I. M. Pinatti, M. Penha, R. F. Gonçalves, L. Gracia, J. Andrés and E. Longo, $ZnWO_4$ nanocrystals: Synthesis, morphology, photoluminescence and photocatalytic properties, *Phys. Chem. Chem. Phys.*, 2018, **20**, 1923–1937.

39 C. Jaramillo-Páez, J. A. Navío, F. Puga and M. C. Hidalgo, Sol-gel synthesis of $ZnWO_4$-(ZnO) composite materials. Characterization and photocatalytic properties, *J. Photochem. Photobiol., A*, 2021, **404**, 112962.

40 D. Barreca, G. Carraro, A. Gasparotto, C. Maccato, T. Altantzis, C. Sada, K. Kaunisto, T. P. Ruoko and S. Bals, Vapor Phase Fabrication of Nanoheterostructures Based on ZnO for Photoelectrochemical Water Splitting, *Adv. Mater. Interfaces*, 2017, **4**, 1–9.

41 Y. Cui, L. Pan, Y. Chen, N. Afzal, S. Ullah, D. Liu, L. Wang, X. Zhang and J. J. Zou, Defected $ZnWO_4$ -decorated WO_3 nanorod arrays for efficient photoelectrochemical water splitting, *RSC Adv.*, 2019, **9**, 5492–5500.

42 L. Al-Farsi, T. M. Souier, M. Al-Hinai, M. T. Z. Myint, H. H. Kyaw, H. M. Widatallah and M. Al-Abri, pH Controlled Nanostructure and Optical Properties of ZnO and Al-doped ZnO nanorod arrays grown by microwave-assisted hydrothermal method, *Nanomaterials*, 2022, **12**, 3735.

43 M. M. Gomaa, G. RezaYazdi, M. Rodner, G. Greczynski, M. Boshta, M. B. S. Osman, V. Khranovskyy, J. Eriksson and R. Yakimova, Exploring NiO nanosize structures for ammonia sensing, *J. Mater. Sci.: Mater. Electron.*, 2018, **29**, 11870–11877.

44 S. Mahajan and S. Jagtap, Metal-oxide semiconductors for carbon monoxide (CO) gas sensing: A review, *Appl. Mater. Today*, 2020, **18**, 100483.

45 T. Nandy, R. A. Coutu and C. Ababei, Carbon monoxide sensing technologies for next-generation cyber-physical systems, *Sensors*, 2018, **18**, 3443.